



Full Length Article

The deteriorated degradation resistance of Mg alloy microtubes for vascular stent under the coupling effect of radial compressive stress and dynamic medium

Mengyao Liu^{a,1}, Yabo Zhang^{a,1}, Qingyuan Zhang^a, Yan Wang^a, Di Mei^{a,b,*}, Yufeng Sun^{a,b},
Liguo Wang^{a,b,c}, Shijie Zhu^{a,b,c,*}, Shaokang Guan^{a,b,c}

^a School of Materials Science and Engineering, Zhengzhou University, Zhengzhou 450001, China

^b Henan Key Laboratory of Advanced Magnesium Alloys, Zhengzhou 450002, China

^c Key Laboratory of Advanced Materials Processing & Mold Ministry of Education, Zhengzhou 450002, China

Received 19 November 2021; received in revised form 2 April 2022; accepted 7 May 2022

Available online xxx

Abstract

The degradation of Mg alloys relates to the service performance of Mg alloy biodegradable implants. In order to investigate the degradation behavior of Mg alloys as vascular stent materials in the near service environment, the hot-extruded fine-grained Mg-Zn-Y-Nd alloy microtubes, which are employed to manufacture vascular stents, were tested under radial compressive stress in the dynamic Hanks' Balanced Salt Solution (HBSS). The results revealed that the high flow rate accelerates the degradation of Mg alloy microtubes and its degradation is sensitive to radial compressive stress. These results contribute to understanding the service performance of Mg alloys as vascular stent materials.

© 2022 Chongqing University. Publishing services provided by Elsevier B.V. on behalf of KeAi Communications Co. Ltd.

This is an open access article under the CC BY-NC-ND license (<http://creativecommons.org/licenses/by-nc-nd/4.0/>)

Peer review under responsibility of Chongqing University

Keywords: Mg alloy; Microtubes; Degradation behavior; Radial compressive stress; Dynamic conditions.

1. Introduction

Mg and its alloys have become the most promising biodegradable metallic materials for biomedical applications due to the outstanding advantages of their mechanical properties, biocompatibility, and biodegradability [1–4]. One of the leading research hotspots of their biomedical application is to manufacture biodegradable vascular stents for solving the permanent retention concerns of the traditional metallic vascular stent in the human body [5,6]. Right now, one type of Mg-based vascular stent from BIOTRONIK (Magmaris®) [7] is commercially available and has been employed in clinical treatment for over thousands of cases. However, several case

reports indicated the consequent restenosis risk of this stent due to its rapid/uneven degradation (in some cases) at the early stage of the service period [8–10], although it has shown safety and effectiveness in the initial small-scale man trials [11]. These facts indicate that the evaluation of biodegradable Mg alloy vascular stents before marketing should be more cautious.

The Mg-based vascular implants are required to have the *in vivo* degradation rate that can be maintained within a certain range to match the entire tissue reconstruction stage [12,13]. Taking into account the ethics and cost issues, *in vitro* corrosion tests, which are typically performed in simulated body fluids, are often used instead of *in vivo* animal trials to select the promising Mg alloys and analyze their degradation behavior during the initial stage of investigations. However, in most cases, the corrosion rates of Mg alloys measured *in vitro* have no apparent relation with their real *in vivo* corrosion rates [14,15]. Apparently, the current frequently employed corro-

* Corresponding authors.

E-mail addresses: dimei@zzu.edu.cn (D. Mei), zhusj@zzu.edu.cn (S. Zhu).

¹ These authors contributed equally to this work

sion evaluation protocols of Mg alloys for biomedical applications are probably not appropriate or representative.

The related literature has noticed that vascular stents serve in the circulatory flow of blood. The flowing liquid generates flowing shear stress, which makes Mg alloys show different corrosion behavior compared to that under static conditions. Mai et al. [16] compared the static corrosion and dynamic corrosion performance of Mg alloys through a self-designed dynamic device. The results showed that the dynamic corrosion rate of Mg alloys was significantly higher than that under static conditions. Media transfer and flowing shear stress caused by the dynamic media are considered as the two main influencing factors for Mg corrosion [17]. According to the research from Hiromoto et al. [18], flowing fluid was believed to prevent the deposition of corrosion products on the surface, resulting in the accelerated corrosion rate of Mg. However, our previous work found that the slow media flow would lead to the decreased corrosion of pure Mg since the continuous supplementary protective media compositions [19]. Liu et al. [20] conducted simulation and experimental works on the degradation of Mg alloy stents in the flowing liquid. It revealed the complex degradation process of Mg alloy caused by the competition relationship between the flow shear stress and the corrosion products in a flowing environment.

Moreover, vascular stents are also subject to stress during the service period. The combined effect of stress and corrosive environment makes Mg alloy vascular stents prone to stress corrosion crack (SCC) and corrosion fatigue (CF), which lead to the premature loss of mechanical properties of Mg alloy stents. Choudhary et al. [21–23] conducted a series of studies on the SCC performance of different Mg alloys, e.g. AZ91D, AZ31D, Mg-Zn-Ca, ZX50, WZ21 and WE43, in simulated physiological solutions. All the results showed that the SCC sensitivity of Mg alloys in the pseudo-physiological environment caused a serious decline in mechanical properties. The mechanism of SCC was considered to be the combination of anode dissolution and hydrogen-induced damage [6,23,24]. Jafari et al. [25] [26] indicated that the initial cracks of SCC and CF started from the localized corrosion regions. Simultaneously, as reported by our previous works [27,28], the alternating stress in the SBF solution also reduced the fatigue life and fatigue strength of the Mg alloy due to the stress corrosion and hydrogen-induced damage. However, it should be emphasized that the vascular stents play a role in propping up the blood vessel wall to restore blood flow. That means the stent is subjected to the radial compressive stress caused by the blood vessel wall. Thus, although the significant influence of stress on Mg corrosion has been generally realized, the normally performed investigations under the tensile stress and alternating axial stress probably cannot accurately reflect the service performances of Mg alloys for vascular stent applications.

The manufacturing process of the Mg-based vascular stent includes two main steps: (i) the fabrication of microtubes by extrusion and drawing; (ii) laser cutting of microtube into stents. It is worth noting that the corrosion performance of Mg alloys is related to the processing technology. Xiong et al.

Table 1
The elemental composition of the Mg-Zn-Y-Nd alloy.

Element	Zn	Y	Nd	Ni	Fe	Cu	Be	Si	Mg
wt.%	2.04	0.44	0.51	0.0013	0.0021	0.0003	0.0001	0.009	Bal.

Table 2
Dimensions of drawing tools, reduction in cross-section area and annealing parameters. (D_0 is the diameters of drawing tools, D_m is the diameter of the mandrel, δ is the thickness of the tube, ψ is the reduction of cross-section area at one pass.)

Pass no.	D_0 / mm	D_m / mm	δ / mm	ψ /%	Annealing conditions
1	2.85	2.45	0.2	11.67	320 °C, 30 min
2	2.80		0.175	13.33	320 °C, 30 min
3	2.75		0.15	15.1	320 °C, 30 min

[29] found that texture evolution caused by plastic deformation changed the corrosion performance of AM80 Mg alloy. Wu et al. [30] processed the Mg-Zn-Y-Nd alloy by cyclic extrusion compression (CEC) and found that both corrosion resistance and mechanical properties of the alloy were improved after processing. Thus, as compared with frequently employed bulk specimens, the performance of microtubes by extrusion and drawing is closer to that of the final stent products [31]. However, this point is not always fully considered in the previous works. For accurately grasping the degradation behavior of Mg-based vascular stents, the corrosion tests of the microtubes should be paid more attention.

The previously published works normally focused on the influence of one specific factor on the degradation behavior of Mg alloys for vascular stent applications, while insufficient attention was paid to the coupling effect of multiple factors. Especially, the influence of radial compressive stress on the degradation of Mg microtubes is rarely mentioned. Therefore, it is of great importance to investigate the degradation behavior of Mg alloy microtubes under radial compressive stress in a flowing medium for further deepening the understanding of the service performance of Mg alloys as vascular stent materials. In this study, the Mg-Zn-Y-Nd alloy was selected to process microtubes [32–34] and the degradation mechanism and change of degradation rate of the microtubes under various flow rates and radial compressive stress were systemically investigated. These findings are helpful for understanding the degradation behavior of Mg implants and provide guidance for the *in vitro* evaluations of Mg-based implants.

2. Experimental

2.1. Materials and processing

The Mg-Zn-Y-Nd alloy, specially designed for vascular stents [35,36], was used in this study. Table 1 lists the detailed elemental composition of this alloy. The manufacturing process of microtubes, which consists of hot extrusion and cold drawing, is shown in Fig. 1(a), which has been reported in our previous studies [32]. The extrusion ratio is 160:1. Table 2 details the cold-drawing and annealing parameters. The

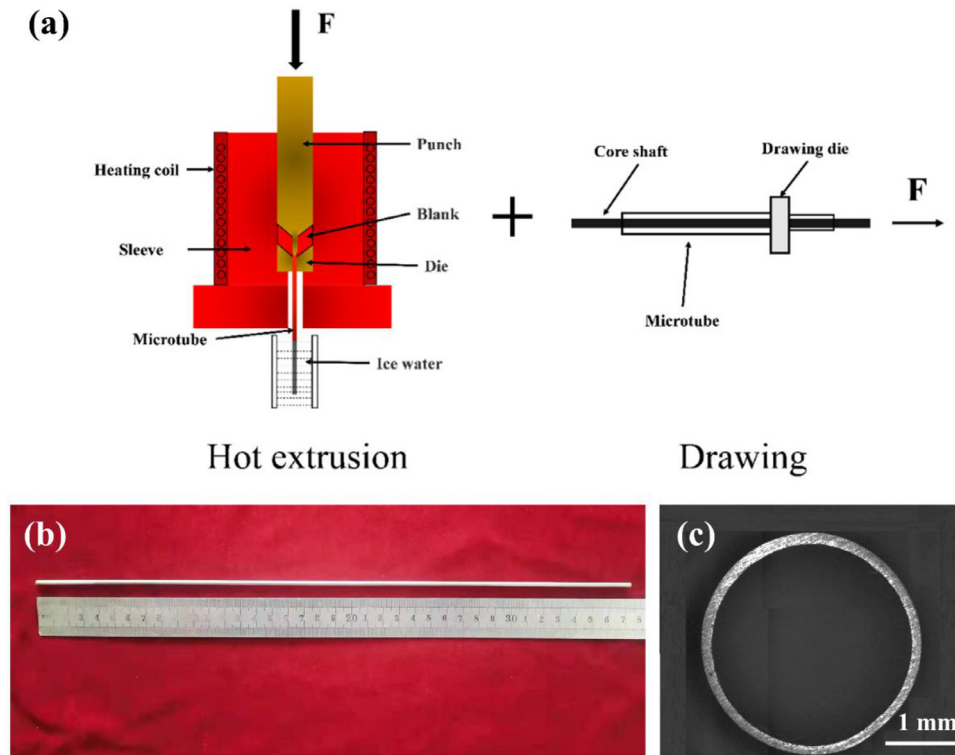


Fig. 1. The schematic of hot extrusion and drawing(a); (b)(c) the shape of magnesium alloy microtube.

microtubes with an outer diameter of about 2.75 mm and a wall thickness of about 0.15 mm were tested, as shown in Fig. 1(b) and Fig. 1(c).

2.2. Microstructure characterization

The specimens for microstructural observation were cut from the longitudinal section and cross-section of microtubes. Those specimens were cold-mounted into the epoxy resin, ground with #100–1000 SiC papers, polished with diamond pastes, and chemically etched by picric acid (2.1 g picric acid + 10 mL acetic-acid + 70 mL methyl-alcohol + 20 mL distilled water). The microstructure of microtube specimens was observed by a Leica DM4000M optical microscopy (OM).

2.3. Mechanical properties test

Tensile and compression tests were conducted at ambient temperature using a universal material test machine (Shimadzu AG-IC) at a displacement rate of $0.5 \text{ mm}\cdot\text{min}^{-1}$ and $0.2 \text{ mm}\cdot\text{min}^{-1}$, respectively. Based on the ISO 6892-1:2009 standard, tensile tube specimens with an overall length of 100 mm and a gage length of 50 mm were used. Two Mg alloy bars (with a length of 25 mm) that matched the inner diameter of microtubes were inserted into the ends of specimens to ensure the proper grip of specimens in the test machine. Referring to the GB/T7314-2017 standard and experimental requirements, 10 mm specimens were used for the compres-

Table 3

Amount of reagents for preparing 1 L of HBSS solution.

Chemical	Amount/ mg	Amount/ mmol
CaCl ₂	140	1.26
MgCl ₂ •6H ₂ O	100	0.49
MgSO ₄ •7H ₂ O	100	0.41
KCl	400	5.33
KH ₂ PO ₄	60	0.44
NaHCO ₃	350	4.17
NaCl	8000	137.93
Na ₂ HPO ₄	48	0.34
D-Glucose	1000	5.56

sion test. Three specimens were tested for each measurement to ensure the reproducibility of the results.

2.4. Degradation test

Hanks' Balanced Salt Solution (HBSS) was chosen to be used in this work. The chemical composition of HBSS is shown in Table 3. A self-designed pressure-induced dynamic degradation test device was employed to perform the degradation test of Mg alloy microtubes in the coupled environment of compressive stress and dynamic flow conditions. The schematic illustration of the test device is shown in Fig. 2. The Mg alloy microtube was placed in a silicone tube, and the inner diameter of the silicone tube is equal to the outer diameter of the microtube. Radial compressive stress was adjusted by rotating the nuts at the ends to move the upper module and the value was monitored by the digital display

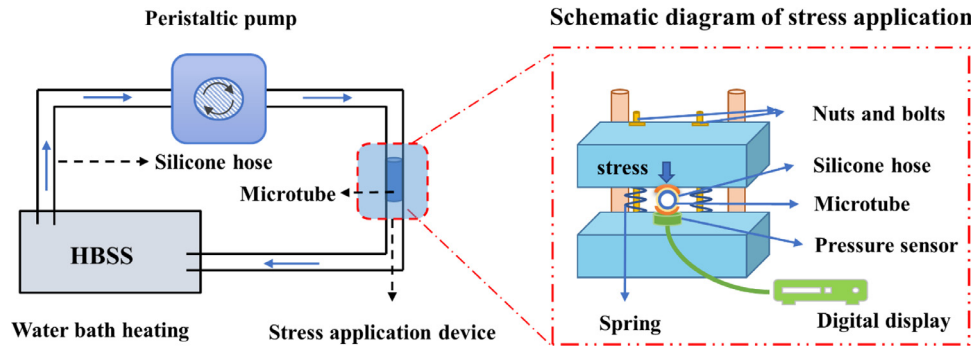


Fig. 2. Schematic of the self-designed pressure-induced dynamic degradation system.

instrument. A peristaltic pump was used to adjust the flow rate of the medium. The solution was maintained at 37°C. Before the degradation test, microtube specimens were firstly electrolytically polished to obtain a smooth and flat surface. Electrolytic polishing was performed at the temperature of $-30\sim-35^{\circ}\text{C}$ by using dry ice. In this work, the degradation behavior of Mg alloy microtubes for the first 90 min's immersion was investigated since the degradation behavior of Mg alloys shows rapid change only at the initial stage of immersion and then becomes stable gradually. The hydrogen collection devices were connected to this system for testing the hydrogen evolution of Mg alloy microtubes. After immersion, the specimens were ultrasonically cleaned with chromic acid for 5 min to remove the corrosion production. The surface morphologies of the corroded specimens were observed by FEI Quanta-200 scanning electron microscopy (SEM) with the accelerating voltage of 20 kV under the secondary electron mode, and the energy dispersive spectroscopy (EDS) was used to analyze the element distribution of the degradation products.

3. Results

3.1. Microstructure and mechanical properties of microtubes

The microstructure of the hot-extruded Mg-Zn-Y-Nd alloy microtube billet is demonstrated in Fig. 3. It shows the fully recrystallized microstructure with an average grain size of around $4.0\ \mu\text{m}$. Since the required wall thickness of the final produced tube is about $100\text{--}150\ \mu\text{m}$, it is better to obtain as small homogeneous grains as possible that can avoid the influence of micro-defects on the corrosion resistance and mechanical properties of the microtubes to a certain extent [37]. However, recrystallization and grain growth occur during the cold-drawing and annealing process which are the subsequent manufacturing processes of stents. Fig. 4 shows the cross-section and longitudinal-section morphologies of the Mg-Zn-Y-Nd alloy microtube with a thickness of 0.15 mm after 30 min of annealing. These phenomena indicate that the extruded refined grains are not retained in the final microtubes.

Fig. 5(a) shows the engineering stress-strain curves of the as-annealed microtubes with an outer diameter of about

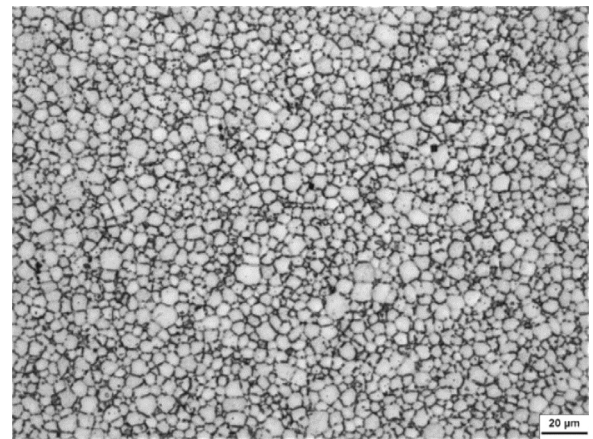


Fig. 3. Microstructure of hot-extruded Mg-Zn-Y-Nd microtube billet.

Table 4
Mechanical properties of Mg-Zn-Y-Nd alloy microtubes.

Specimen	YS(MPa)	UTS(MPa)	Elongation(%)
Tensile microtubes	212 ± 2	295 ± 3	$15.7 \pm 0.3\%$

2.75 mm and a wall thickness of about 0.15 mm. The yield strength (YS), ultimate tensile strength (UTS), and elongation are summarized in Table 4. The radial support force test of the microtubes is crucial for the selection of the compression stress parameters of the degradation tests under compressive stress. Fig. 5(b) shows the radial support stress-strain curve of the microtube specimen with a length of 10 mm. Unlike the round rod specimens, the radial support stress of the hollow tube that is not allowed to be deformed is small. In this work, the maximum stress value of elastic deformation is $2.3 \pm 0.3\ \text{MPa}$, corresponding to a force of $7.2 \pm 0.8\ \text{N}$. Therefore, in the following experiments, the pressure value for the degradation test of microtube specimens under stress is less than this value.

3.2. The dynamic corrosion behavior of microtubes

The degradation rates of Mg alloy microtubes with a length of 10 mm were measured by weight loss and hydrogen evolution in HBSS under dynamic conditions with various flow

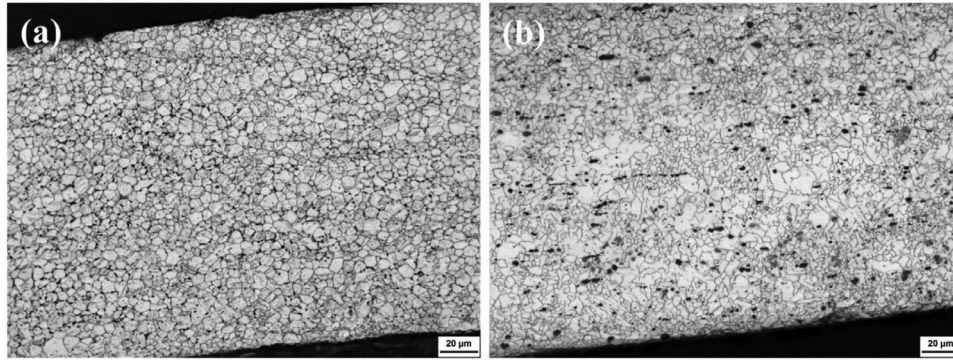


Fig. 4. Cross-section (a) and longitudinal section (b) microstructure of Mg-Zn-Y-Nd alloy microtube with the thickness of 0.15 mm after 30 min annealing.

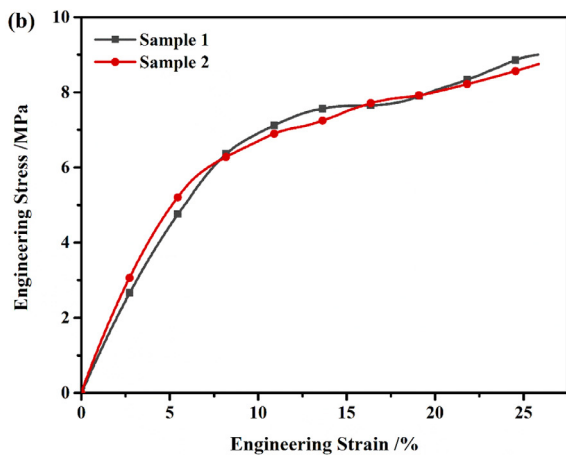
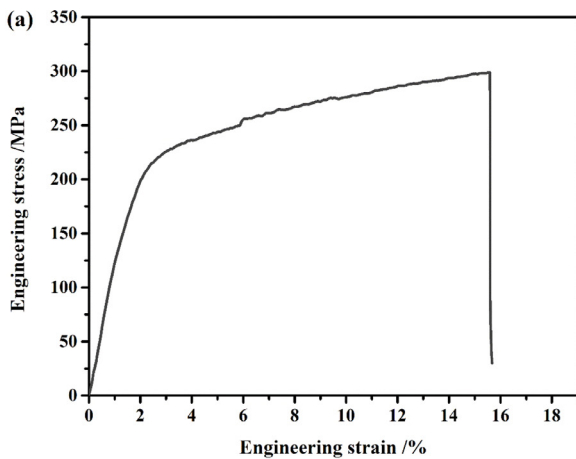


Fig. 5. Typical tensile (a) and radial support stress (b) curve of Mg-Zn-Y-Nd alloy microtubes.

rates of 0–30 mL·min⁻¹ during 90 min immersion period, as shown in Fig. 6. It could be found that the degradation of microtube accelerates with the increase of flow rate. This finding corresponds well with the previously reported work [38]. Wang et al. [39] also elaborated on this point that the corrosion rate of Mg alloy increased due to the localized, pitting and erosion mechanisms caused by high-speed flow. The morphologies of corroded Mg-Zn-Y-Nd microtubes were

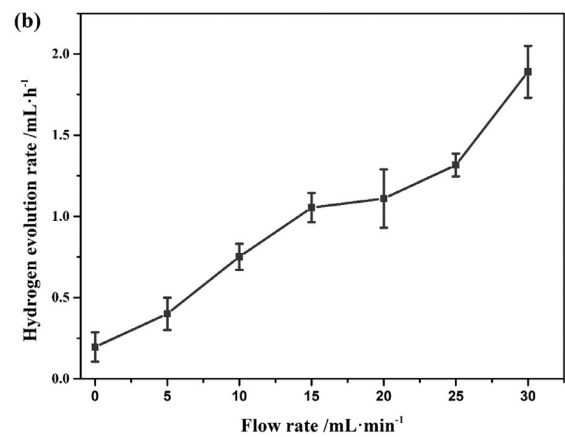
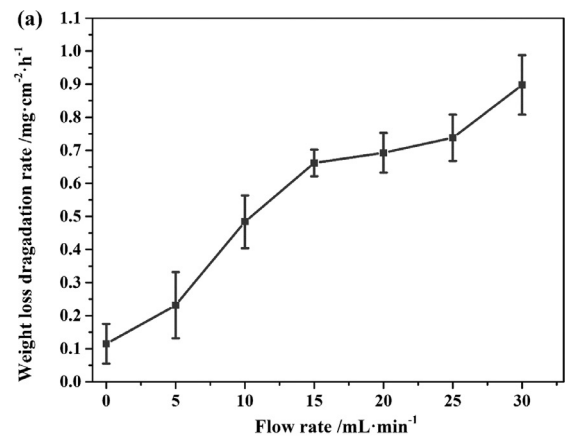


Fig. 6. The degradation rate of the Mg-Zn-Y-Nd microtubes in HBSS solution with different fluid flow rates: (a) weight loss degradation rate; (b) hydrogen evolution rate.

observed by SEM, which are shown in Fig. 7 (the image of each tube was spliced by multiple SEM images). It could be found that the cluster-like corrosion products cover the surface of the microtube which was immersed in the static medium. The precipitation of degradation products isolates the contact between the Mg substrate and the test media [40]. In the case of dynamic tests with a relatively higher flow rate, the flow shearing stress generated by the dynamic medium moves the partial corrosion products away from the surface of micro-

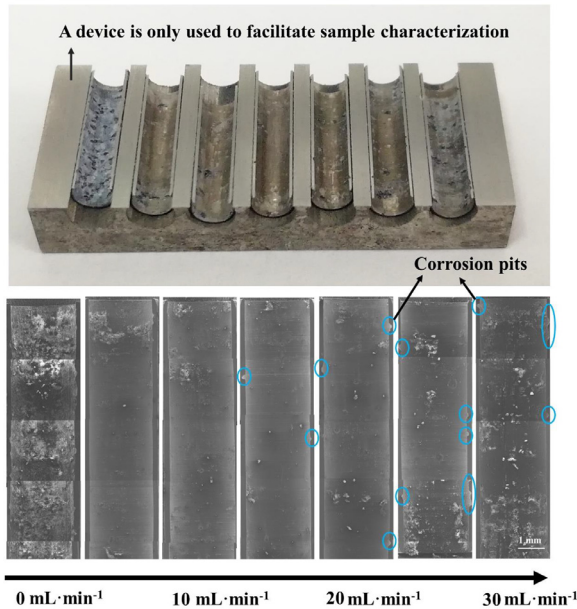


Fig. 7. Morphologies of corroded Mg-Zn-Y-Nd alloy microtubes under different flow rates (the picture of each microtube was formed by stitching multiple SEM pictures).

tubes [20], which accelerates the degradation of microtubes. Fig. 8 shows the elemental distribution of corrosion products formed on the microtube after 90 minutes' immersion in the dynamic HBSS with the flow rate of $15 \text{ mL}\cdot\text{min}^{-1}$. Although its surface morphology does not show the accumulation of a large number of cluster-like corrosion products, its cross-section morphology confirms the formation of the Ca-P corrosion products layer in the dynamic medium. The flow shear stress takes away the cluster corrosion products, which are weakly bonded to the surface but will not expose the matrix entirely. This feature corresponds well to the results of the abovementioned weight loss and hydrogen evolution test. With the increase of flow rate, corrosion pits gradually appear (Fig. 7). Once small pits with a height difference from

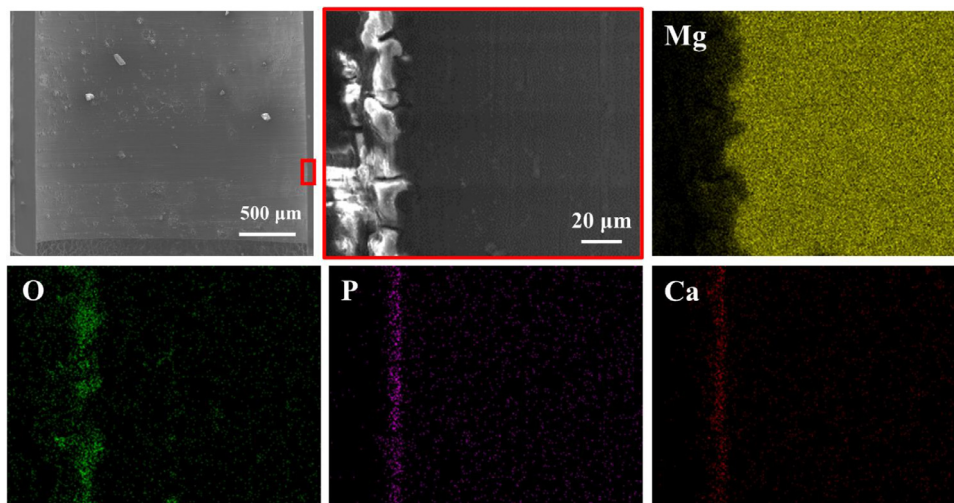


Fig. 8. The elements distribution of corrosion products on Mg microtubes in HBSS solution under the flow rate of $15 \text{ mL}\cdot\text{min}^{-1}$.

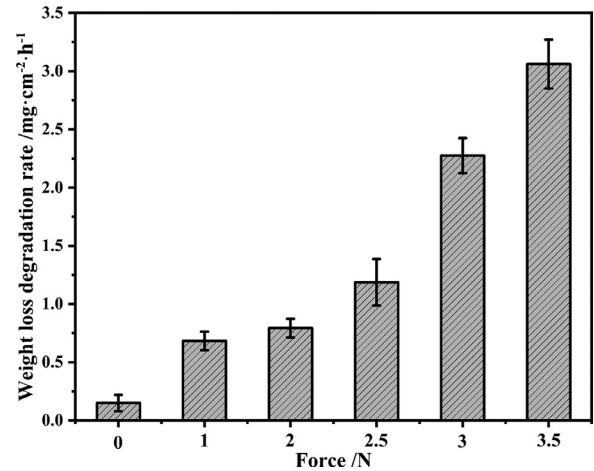


Fig. 9. Weight loss degradation rate of Mg-Zn-Y-Nd alloy microtubes under different stress conditions in dynamic HBSS with $10 \text{ mL}\cdot\text{min}^{-1}$ flow rate at $37 \text{ }^\circ\text{C}$ for 90 min.

the base surface appear, the flow shear stress can conveniently remove the corrosion products on the surface instead of that in the corrosion pits. It weakens the uneven localized corrosion of Mg alloy microtubes to a certain extent.

3.3. The dynamic corrosion performance under radial compressive stress

According to the radial support force curve of microtubes (Fig. 5(b)), the radial compressive force with the range of 0–3.5 N was loaded on microtubes to investigate the degradation behavior of Mg microtubes under the coupling effect of dynamic medium and compressive stress. In this section, the flow rate of the medium was kept at $10 \text{ mL}\cdot\text{min}^{-1}$ for focusing on the influence of compressive stress. As shown in Fig. 9, the degradation rate of microtubes in HBSS under dynamic conditions increases along with the increase of stress. The results show that the degradation rate of microtubes un-

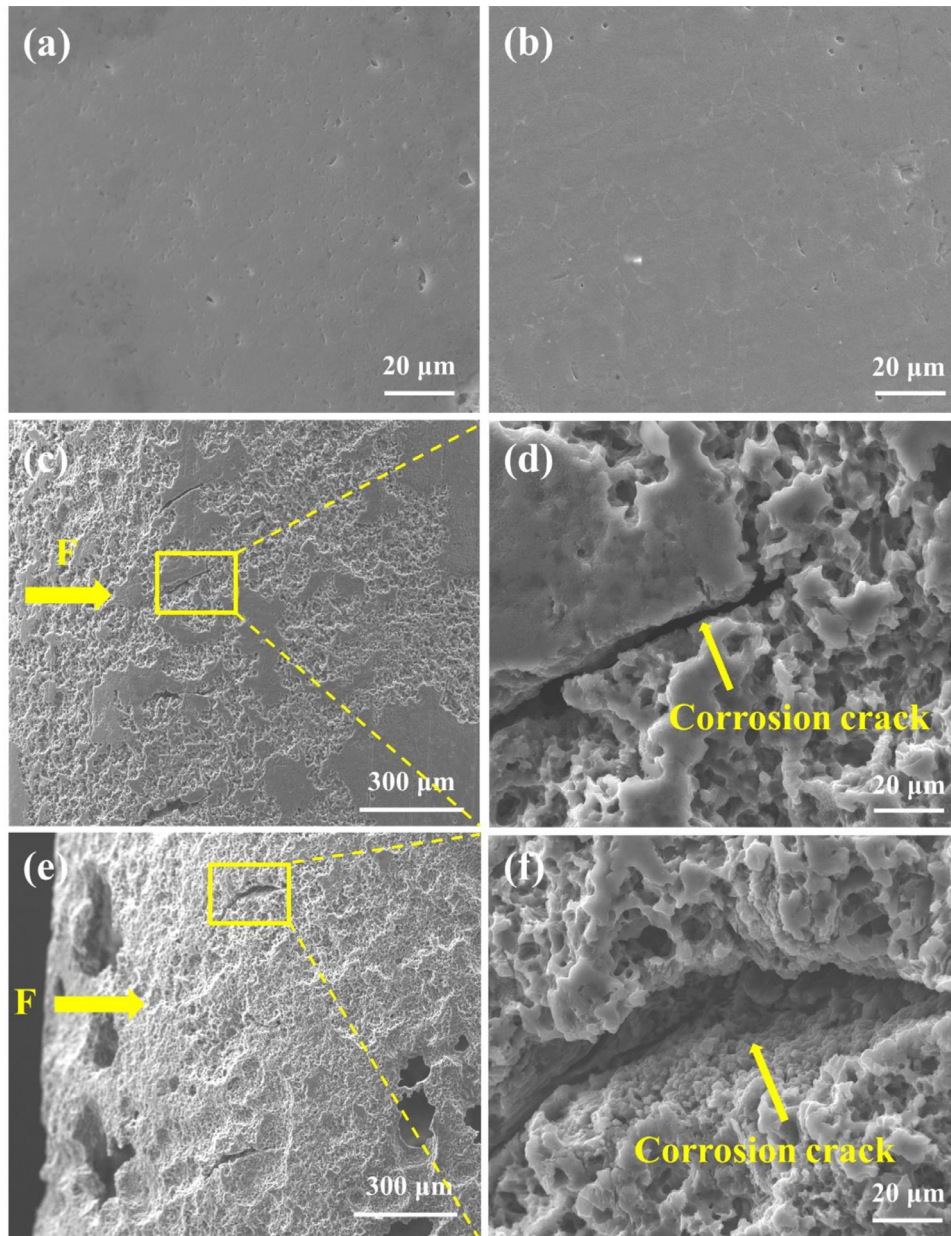


Fig. 10. The corrosion morphologies of the outer surface for Mg–Zn–Y–Nd alloy microtubes after removing corrosion products under different stress conditions in dynamic HBSS with the flow rate of $10 \text{ min} \cdot \text{mL}^{-1}$ at $37 \text{ }^\circ\text{C}$ for 90 min. (a) 0; (b) 1 N; (c)(d) 2 N; (e)(f) 3.5 N.

der stress conditions of 1 N is about 7 times higher than that under stress-free conditions. However, from 1 N to 2 N, the degradation rate of microtubes has no significant change. When the pressure increases to over 2 N, the dynamic corrosion rate shows a sharp increase. The results confirm that the introduction of compressive stress significantly accelerates the degradation of the microtubes.

The morphologies of the outer surface without corrosion products after testing under varying stress conditions are shown in Fig. 10. Although the microtube and the external silicone tube fit well, a small amount of liquid still penetrates between the tube wall and the silicone tube due to the effect of the applied stress or the corrosion holes. The morphologies indicate that the microtubes corrode violently as the stress in-

creases. Under stress-free conditions, as shown in Fig. 10(a), the corroded microtubes have a flat surface without any perforations. It has been confirmed that the α -Mg phase acts as the anode during the corrosion process in most cases [41], which is preferentially corroded, resulting in the detachment of the second phases and the formation of small holes/pits. The morphology of microtubes corroded under 1 N force exhibits the features of intercrystalline corrosion (Fig. 10(b)). The slipping of grain boundary under stress is one of the deformation mechanisms of metallic materials [42]. Stress acting on microtubes increases the grain boundary energy, leading to intercrystalline corrosion. When the loading force is 2 N, corrosion cracks appear on the surface of microtubes. Fig. 10(c) and (d) show that narrow corrosion cracks expand along the axial and

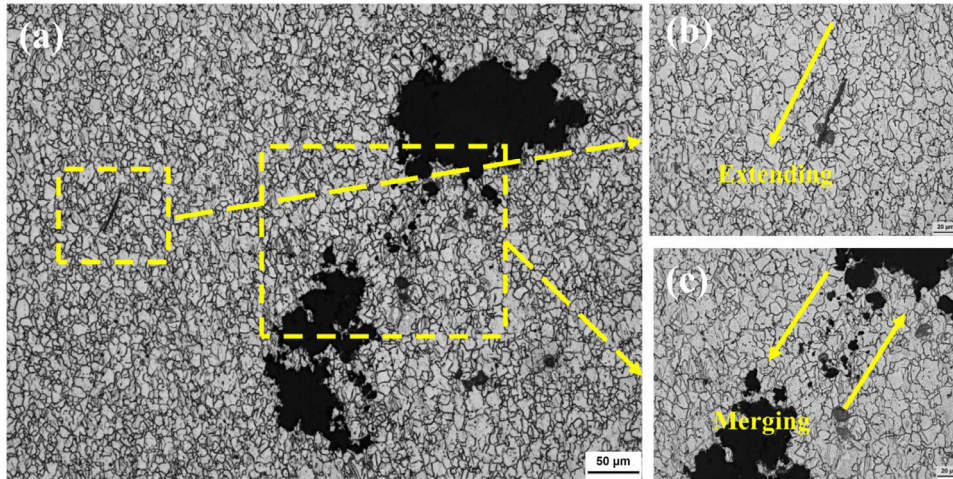


Fig. 11. (a) Global and (b)(c) local surface microstructure of Mg-Zn-Y-Nd alloy microtube after 90 min's immersion at 2 N with $10 \text{ min} \cdot \text{mL}^{-1}$ flow rate.

radial direction with the deepening of adjacent corrosion pits. As the loading force increases from 2 N to 3.5 N, corrosion cracks become wider and deeper (Fig. 10(e) and (f)). Significantly, the corrosion pits expand and eventually penetrate the wall of microtubes. In addition, hydrogen is generated during the degradation of Mg microtubes, which contributes to the propagation of corrosion cracks and causes hydrogen-induced damage under stress [24,43]. The above reasons lead to severe corrosion and ultimate failure of microtubes.

Due to the application of stress, a special phenomenon also appeared. Fig. 11 shows the microstructure of the Mg alloy microtube after dynamic corrosion under the loading force of 2 N. A corrosion crack with a length of about $50 \mu\text{m}$, a few sporadic corrosion pits and two big corrosion pits exhibit in Fig. 11(a). The increased grain boundary energy causes the extension of corrosion cracks along the grain boundaries at the initial stage (Fig. 11(b)) [42,44]. During the corrosion process of Mg alloy, corrosion pits expand in the form of grain peeling layer by layer because of the dissolving of the anodic Mg matrix. Annexation and fusion lead to the growth of corrosion pits. Under the combined action of corrosive medium and compressive stress, two large corrosion pits show a tendency to merge, Fig. 11(c).

3.4. The corrosion crack of microtubes

The application of stress often leads to cracks. Fig. 12 reveals the microstructure of the corrosion crack on the Mg alloy microtube after 90 min's dynamic corrosion under the loading force of 2.5 N. Both transgranular and intergranular crack propagation appear in Fig. 12(b). It fits with the previous analysis. For this alloy, the application of compressive stress can activate the grain boundaries and easily form intergranular corrosion cracking cracks. Farther, hydrogen is generated and accumulated during Mg corrosion [45]. It has been proved that the hydrogen-induced crack of Mg alloys is transgranular stress corrosion cracking (TGSCC) [46]. Therefore, the influence of hydrogen should be taken into account in our case. In this coupled environment, flow shear stress re-

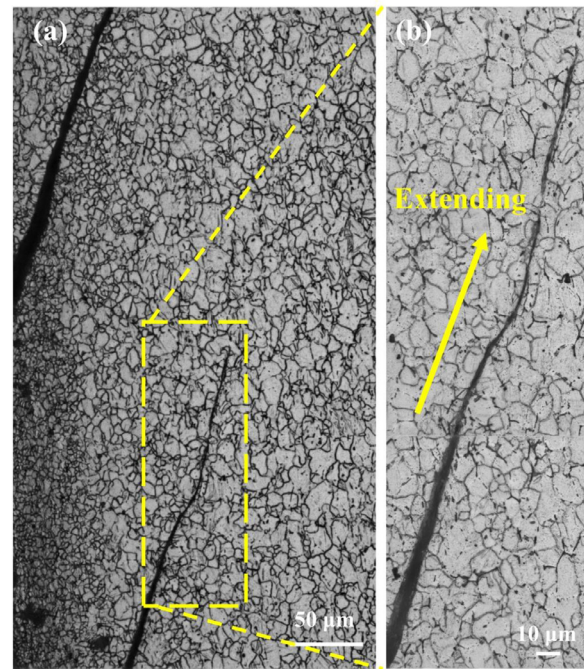


Fig. 12. Microstructure of corrosion crack on Mg-Zn-Y-Nd alloy microtubes after dynamic corrosion for 90 min at 2.5 N with $10 \text{ min} \cdot \text{mL}^{-1}$ flow rate.

moves corrosion products to accelerate corrosion. Once tiny corrosion defects occur, the crack is easy to form and gradually expands under the action of stress. Due to the existence of hydrogen and high-energy grain boundaries, the cracks of Mg-Zn-Y-Nd microtubes alloy are featured by a mixed mode of transgranular and intergranular cracking.

4. Discussion

4.1. The influence of specimen shape on mg degradation

Typically, bulk samples have been employed in previous studies for investigating the degradation performance of Mg

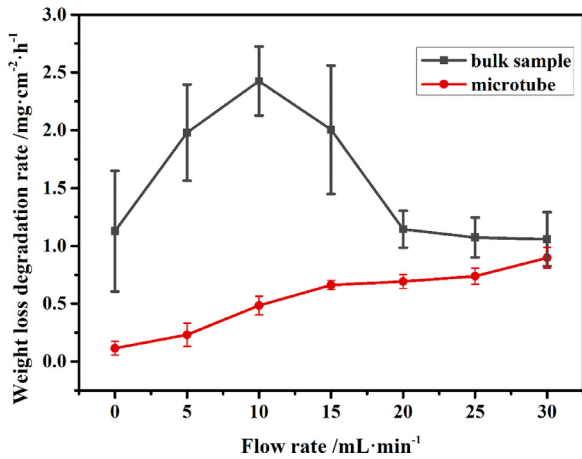


Fig. 13. The weight loss degradation rate of Mg-Zn-Y-Nd alloy with different shapes.

alloys for biomedical applications. In this work, the Mg alloy microtubes were tested for analyzing the influence of flow rate and radial compressive stress on Mg degradation. Fig. 13 compares the degradation rate of bulk Mg specimens and Mg microtubes in the dynamic HBSS with various flow rates. The results show that the bulk specimens with an exposed surface of 9 mm×10 mm (similarly, the exposed surface is parallel to the extrusion direction) have higher degradation rates in HBSS as compared to that of microtubes under the same conditions.

Differ from that of microtubes, the degradation rate of bulk specimens shows no positive correlation with the increase of flow rate. Under the action of the flowing fluid, due to the large diameter (almost 10 mm) of the experimental chamber for the bulk samples, the actual flow shear stress is much smaller than the shear stress received by the microtubes at the same flow rate. In addition, the bigger chamber is beneficial for the stabilization of the corrosive environment. Influencing by the above factors, with the increase of flow rate, the corrosion rate of the bulk samples increases firstly, then decreases, and finally remains stable. There is no doubt that processing procedures from billets to microtubes change the microstructure of the Mg materials and then affect their degradation rate. More importantly, in our case, the specimen shape also significantly affects the degradation behavior of Mg alloy. On the one hand, the specimen shape influences the flowing fluid of the medium and then affects the flow shear stress which is believed to have a significant influence on Mg corrosion [47]. On the other hand, the thin-wall and hollow structure of microtube lead to completely different degradation features compared to that of bulk specimens of Mg alloys. For example, the localized corrosion of microtubes will penetrate the wall of microtubes and lead to the premature and complete loss of their mechanical integrity, but it shows a less significant influence on that of bulk specimens.

Based on our results, it could be found that different specimen shape causes different research results about the degradation rate of Mg alloys. Therefore, in order to obtain research

results closer to the real service state, when the tests are performed under dynamic conditions, it was suggested that the specimen shape should be ensured to be consistent and as close as possible to the shape of the final products.

4.2. The influence of dynamic flow and stress on the degradation of mg microtubes

Han et al. [38] revealed that fluid corrosion is mainly related to the corrosion process of the surface layer, which is affected by flow shear stress and medium transfer. Although our previous work found that the flowing fluid is beneficial for stabilizing the medium environment [19], but the high flow rate hinders the deposition of the corrosion products, and also promotes the shedding of the corrosion product layer. Fig. 14 shows the simulation results of the real flow rate during the measurements under the dynamic conditions with different input flow rates. The results indicate that the presence of microtubes changes the flow rate in the around areas and the real flow rate near the inner surface of the microtube is significantly higher than the preset rate. Especially, the different flow rates around the ends and the middle of the microtube indicate the different flow shear stress at different locations, resulting in the inhomogeneous degradation of the microtubes. It is reasonable to assume that the vascular stents with more complex structure would have a more significant influence on the hemodynamics in vascular and then feedback affects the degradation behavior of Mg stents.

As abovementioned in the introduction section, the influence of stress on Mg degradation has been noticed in much literature. However, the typically employed tensile/compressive stress and alternating axial stress cannot reflect the true force state of Mg implants in the vascular vessel. In fact, under different stress states, the causes of stress corrosion/corrosion fatigue cracks in Mg alloys are also different. It is generally believed that materials subjected to axial compressive stress are not prone to stress corrosion [48]. Under the action of axial tensile stress and alternating stress, the galvanic corrosion between the second phase/impurities and the matrix and the peeling of the corrosion products by the action of stress lead to the initiation of cracks. In this work, the crack initiation of microtubes under the action of radial compressive stress is mainly derived from the galvanic corrosion caused by the potential difference between the second phase/impurities and the substrate and the increased grain boundary energy. Thus, as emphasized by Li et al. [49], in order to deepen the understanding of the service performance of Mg alloy vascular stents, it is important to conduct degradation tests of Mg alloys under realistic loadings.

4.3. The corrosion mechanism of microtubes under the coupling effect

The degradation behavior of Mg alloy microtubes under the coupling effect of radial compressive stress and dynamic media is described by the schematic diagram that is shown in Fig. 15. The static corrosion process of microtubes is

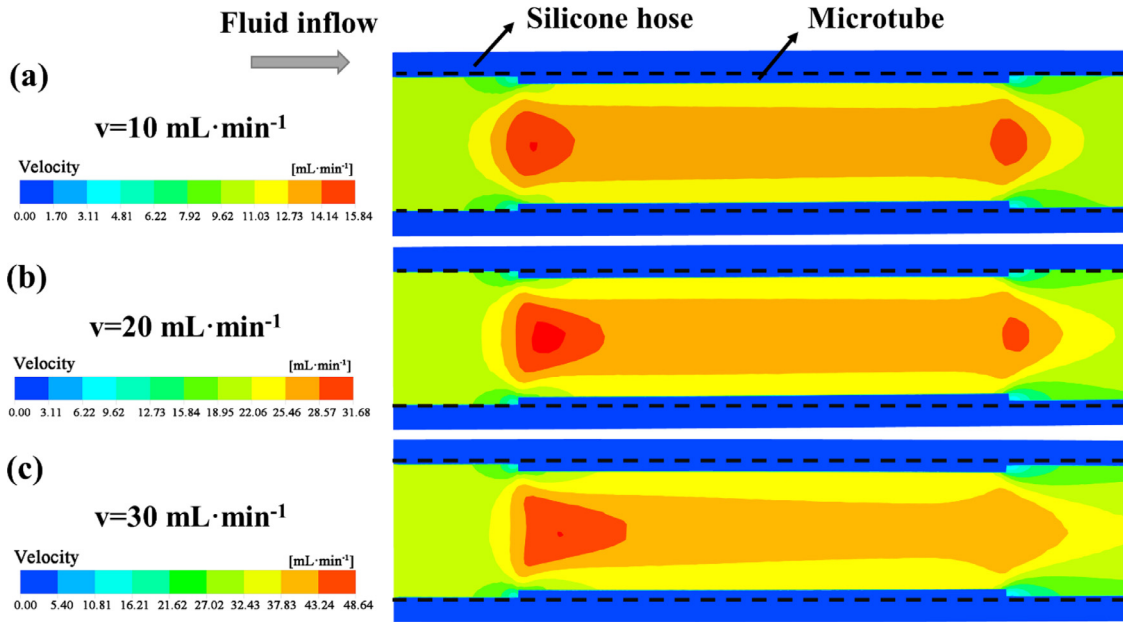


Fig. 14. The simulation results of the real flow rate during the measurements under the dynamic conditions with different input flow rates. (a) $10 \text{ mL}\cdot\text{min}^{-1}$; (b) $20 \text{ mL}\cdot\text{min}^{-1}$; (c) $30 \text{ mL}\cdot\text{min}^{-1}$.

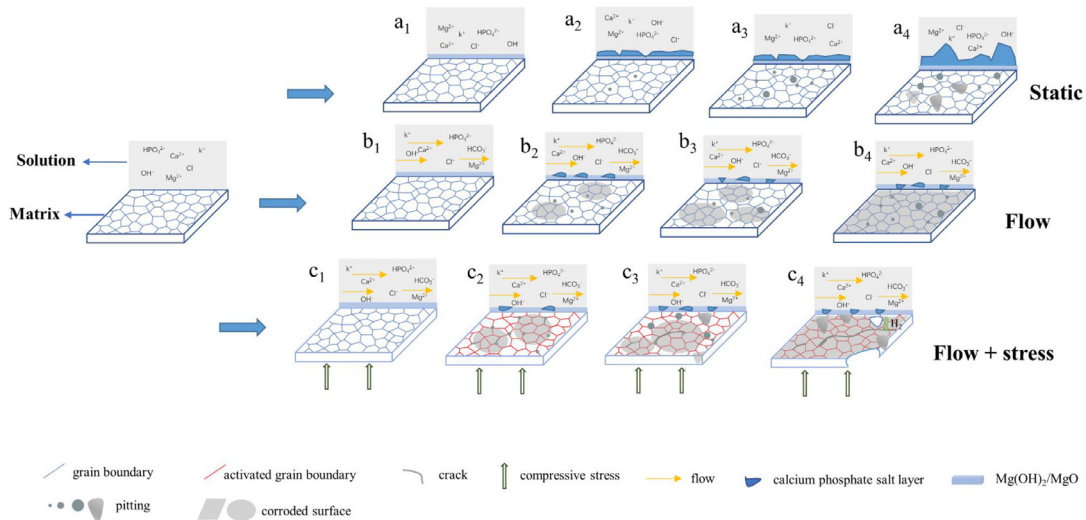


Fig. 15. Schematic illustration of the degradation behavior of the Mg microtubes under different environments.

relatively simple and has been reported [32,34]. As shown in Fig. 15(a), due to the effect of galvanic corrosion between the Mg matrix and second phases (or impurities), corrosion pits will gradually appear. The galvanic corrosion also promotes the formation of the protective corrosion products (Fig. 15(a2)), containing the outer calcium phosphate salt deposit protective layer and inner porous $\text{Mg}(\text{OH})_2/\text{MgO}$ layer, on the surface of microtubes during the immersion period in HBSS [40]. However, these partially protective corrosion products cannot completely isolate the contact between the substrate and the medium. The Mg substrate continues to corrode, and the corrosion product layer gradually thickens (Fig. 15(a4)). Thanks to the less corroded area, the corrosion rate of microtubes under this condition is the lowest. The

formation process of the protective layer on the Mg surface is precipitation/deposition dominant [40]. Thus, it can be removed from the surface of the substrate by the flow shear stress.

Under the dynamic conditions, as shown in Fig. 7 and Fig. 15(b), there are a few Ca-P clusters formed on the surface of the microtube and they are majority retain in the corrosion pits. In this case, although the bigger and deeper corrosion pits cannot be formed, there still have a higher corrosion rate. It has been confirmed that the local environment near the corroding specimen surface is different from the bulk medium environment during the static immersion test [50]. Under static conditions, the medium near the inner wall of the hollow microtubes cannot be renewed in time. Although the

increased OH^- near the inner wall area promotes the precipitation of partially protective products and thereby inhibiting the corrosion of Mg microtubes to a certain extent, the formation of protective corrosion products consumes the medium components, which is unbeneficial for the long-term protection. Two main factors of dynamic media affect the degradation of microtubes, namely flow shear stress and medium renewal [17]. The dynamic environment with a low flow rate helps to stabilize the medium composition around the sample. In HBSS-like media, a stable medium composition is essential for the continuous formation of protective precipitation products. In our previous work, it has been found that the dynamic medium with a flow rate of $0.5 \text{ mL}\cdot\text{min}^{-1}$ would not disturb the sample surface, but the stable medium environment leads to a decreased corrosion rate of commercial pure Mg [19]. As the flow rate gradually increases, the flow shear stress takes away the protective precipitation products on the surface of the microtubes, resulting in an increase in the corrosion rate and overall corrosion of the surface of Mg alloy microtubes (Fig. 15(b4)). However, the accelerated corrosion brings an excess of OH^- , which in turn promotes the formation of precipitated products. As shown in Fig. 6, with the increase of flow rate from 15 to $20 \text{ mL}\cdot\text{min}^{-1}$ (for hydrogen evolution) and $15\text{--}25 \text{ mL}\cdot\text{min}^{-1}$ (for weight loss), the corrosion rate of microtubes does not show significant change. It corresponds well with the aforementioned multifactorial antagonism effect of flow rate on the corrosion rate of Mg alloy microtube.

The coupled stress field makes the degradation behavior of microtubes more complicated, and the corrosion rate is further significantly accelerated. In addition to the factors mentioned above, the compressive stress activates the grain boundary and increases the energy of the grain boundary, which promotes the preferential occurrence of corrosion around the high-energy grain boundaries area [42]. Pinhole pits develop along the crystal form corrosion cracks under stress (Fig. 15(c2)). The generated hydrogen participates in the crack growth. The propagation mode of the cracks is in the manner of a mixed-mode, consisting of stress and hydrogen-induced damage. The grains are more likely to fall off under the action of flow shearing stress. A final consequence is that the microtube wall is corroded into a perforation, and cracks break the structural integrity by propagating (Fig. 15(c4)). The influence of the application of radial compressive stress on the degradation rate of microtubes is not linear (Fig. 10). Similar to the influence of flow rate, the degradation of Mg microtubes under radial compressive stress in the dynamic medium is also affected by the multifactorial antagonism effect. The stress accelerates the corrosion of Mg microtubes, but the accelerated corrosion promotes the precipitation of partially protective products. This makes the degradation rate of Mg microtubes with the increase of stress under a certain range (from 1 N to 2 N) shows less change.

4.4. Outlooks

The complex environment of the human body makes it hard to find a suitable test environment to simulate the ser-

vice environment of a stent. There is still controversy regarding the evaluation test methods for Mg-based implants in the community so far, which makes the experimental results from different groups less comparable and referential [51]. In the previous work on the evaluation of *in vitro* degradation behavior of biodegradable Mg alloys for vascular stents, it was mainly focused on the influence of alloy composition and deformation processing on their degradation behavior, while insufficient attention was paid to the influence of test conditions. Our previous work found that the choice of corrosion test medium composition has a significant impact on the degradation behavior of Mg alloys [50,52]. In this work, it was found that different sample shapes also cause differences in test results. The exhibited degradation rate of Mg alloy microtubes is not related to that of the frequently employed bulk material, while the shape of the former one is closer to the final product. More importantly, it was tried to introduce a radial compressive stress model that is closer to the actual service environment of Mg vascular stents to deepen the understanding of the degradation behavior of Mg microtubes, which is rare in the previous related studies. The research results finally confirmed that the selection of the appropriate stress mode is very critical for the research of stress-induced Mg degradation.

However, although the introduced degradation test environment of Mg alloy microtubes (under the coupling effect of radial compressive stress and dynamic medium) in this work is closer to the service environment of the stent than the frequently employed test environment before, it remains incompletely correlated to the real stress state of the stent in the blood vessel. The periodic beating of the heart causes the blood to flow in a pulsed form rather than a constant current state. Thus, the actual flow shear stress experienced by the stent changes periodically. In addition, the pulsed blood also causes the periodic contraction and expansion of the blood vessel, resulting in the periodical changing of the radial stress on the stent during the service period. Differ from the simple constant stress, this coupled alternating stress environment places higher demands on material properties, such as corrosion fatigue, and mechanical integrity. We have to admit that it is not easy to fully simulate the real service environment of vessel implants in the human body. However, it is still necessary to further optimize the *in vitro* test environment and make the experimental results of degradation tests more informative.

5. Conclusions

The degradation behavior of Mg alloy microtubes under radial compressive stress and dynamic flow conditions is investigated in this work. The following conclusions were drawn based on the research results:

- (1) The degradation rate of Mg alloy microtubes increases with the flow rate. The competitive relationship between flow shear stress generated by the fluid and corrosion

product precipitation ultimately dominates the degradation rate of Mg alloy microtubes.

- (2) Mg alloy microtubes show greater sensitivity to radial compressive stress. The higher corrosion rate is due to the fusion of corrosion pit, shedding of grains, and the generation and propagation of microcracks caused by radial compressive stress.
- (3) The corrosion cracks propagation of Mg alloy microtubes is carried out in the way of intergranular cracking and transgranular cracking influenced by the combination of stress and hydrogen.
- (4) Compared with other stress modes, the introduction of radial compressive stress can better simulate the actual stress environment of Mg alloy vascular stents during service. The *in vitro* evaluation of the degradation behavior of Mg alloy microtubes under the coupling effect of radial compressive stress and dynamic medium is beneficial for the deep understanding of the degradation behavior of Mg-based vascular implants.

Declaration of Competing Interest

This piece of the submission is being sent via mail.

Data availability

The raw/processed data required to reproduce these findings cannot be shared at this time as the data also forms part of an ongoing study.

Acknowledgments

The authors thank the financial support of the [National Key Research and Development Program of China \(2018YFC1106703\)](#) and the Key Projects of the Joint Fund of the [National Natural Science Foundation of China \(U1804251\)](#).

Reference

- [1] G. Uppal, A. Thakur, A. Chauhan, S. Bala, J. Magn. Alloys (2021), doi:[10.1016/j.jma.2021.08.017](#).
- [2] D. Mei, C. Wang, M. Nienaber, M. Pacheco, A. Barros, S. Neves, R.L. Reis, S. Zhu, J. Bohlen, D. Letzig, S. Guan, M.L. Zheludkevich, S.V. Lamaka, Corros Sci 189 (2021) 109567, doi:[10.1016/j.corsci.2021.109567](#).
- [3] N. Sezer, Z. Evis, M. Koç, J Magn Alloys 9 (2021) 392–415, doi:[10.1016/j.jma.2020.09.014](#).
- [4] N. Sezer, Z. Evis, S.M. Kayhan, A. Tahmasebifar, M. Koc, J. Magn. Alloys 6 (2018) 23–43, doi:[10.1016/j.jma.2018.02.003](#).
- [5] L. Aljihmani, L. Alic, Y. Boudjemline, Z.M. Hijazi, B. Mansoor, E. Serpedin, K. Qaraqe, J Bio- Tribo-Corros 5 (2019) 26, doi:[10.1007/s40735-019-0216-x](#).
- [6] S. Jafari, S.E. Harandi, R.K. Singh Raman, JOM 67 (2015) 1143–1153, doi:[10.1007/s11837-015-1366-z](#).
- [7] BIOTRONIK, in, <https://www.biotronik.com/en-de/products/coronary/magmaris>.
- [8] T.Ø. Barkholt, O. Neghabat, C.J. Terkelsen, E.H. Christiansen, N.R. Holm, Circulation 10 (2017) e005677, doi:[10.1161/CIRCINTERVENTIONS.117.0056](#).
- [9] T. Marynissen, K. McCutcheon, J. Bennett, Catheter Cardiovasc Interv 92 (2018) 310–312, doi:[10.1002/ccd.27676](#).
- [10] H. Yang, F. Zhang, J. Qian, J. Chen, J. Ge, JACC: Cardiovasc Interventions 11 (2018) e77–e78, doi:[10.1016/j.jcin.2018.02.040](#).
- [11] M. Haude, H. Ince, A. Abizaid, R. Toelg, P.A. Lemos, C. von Birgelen, E.H. Christiansen, W. Wijns, F.J. Neumann, C. Kaiser, Lancet North Am Ed 387 (2016) 31–39, doi:[10.1016/S0140-6736\(15\)00447-X](#).
- [12] Y.F. Zheng, Y. Wu, Acta Metall Sinica 53 (2017) 257–297, doi:[10.11900/0412.1961.2016.00529](#).
- [13] Y.F. Zheng, H.T. Yang, Acta Metall Sinica 53 (2017) 1227–1237, doi:[10.11900/0412.1961.2017.00270](#).
- [14] A. Atrens, S. Johnston, Z.M. Shi, M.S. Dargusch, Scr Mater 154 (2018) 92–100, doi:[10.1016/j.scriptamat.2018.05.021](#).
- [15] A.H. Martinez Sanchez, B.J.C. Luthringer, F. Feyerabend, R. Willumeit, Acta Biomater 13 (2015) 16–31, doi:[10.1016/j.actbio.2014.11.048](#).
- [16] E.D. Mai, H. Liu, Progr Natl. Sci 24 (2014) 554–560, doi:[10.1016/j.pnsc.2014.08.012](#).
- [17] T. Zhu, Y. Yu, J. Yang, Y.S. Shen, L.Y. He, Y. Xiong, Mater Chem Phys 259 (2021) 124039, doi:[10.1016/j.matchemphys.2020.124039](#).
- [18] S. Hiromoto, A. Yamamoto, N. Maruyama, H. Somekawa, T. Mukai, Corros Sci 50 (2008) 3561–3568, doi:[10.1016/j.corsci.2008.09.0](#).
- [19] D. Mei, C. Wang, S.V. Lamaka, M.L. Zheludkevich, J Magn Alloys 9 (2021) 805–817, doi:[10.1016/j.jma.2020.07.002](#).
- [20] D.X. Liu, S.W. Hu, X.Y. Yin, J.J. Liu, Z. Jia, Q.L. Li, Materials Science & Engineering C 84 (2018) 263–270, doi:[10.1016/j.msec.2017.12.001](#).
- [21] L. Choudhary, J. Szmeling, R. Goldwasser, R.K. Singh Raman, Procedia Eng 10 (2011) 518–523, doi:[10.1016/j.proeng.2011.04.087](#).
- [22] L. Choudhary, R.K. Singh Raman, Eng Fract Mech 103 (2013) 94–102, doi:[10.1016/j.engfracmech.2012.09.016](#).
- [23] L. Choudhary, R.K. Singh Raman, J. Hofstetter, P.J. Uggowitzer, Mater Sci Eng C 42 (2014) 629–636, doi:[10.1016/j.msec.2014.06.018](#).
- [24] R.G. Song, C. Blawert, W. Dietzel, A. Atrens, Mater Sci Eng, A 399 (2005) 308–317, doi:[10.1016/j.msea.2005.04.003](#).
- [25] S. Jafari, R.K. Singh Raman, C.H.J. Davies, Eng Fract Mech 137 (2015) 2–11, doi:[10.1016/j.engfracmech.2014.07.007](#).
- [26] S. Jafari, R.K.S. Raman, C.H.J. Davies, J. Hofstetter, P.J. Uggowitzer, J.F. Loffler, J Mech Behav Biomed Mater 65 (2017) 634–643, doi:[10.1016/j.jmbbm.2016.09.033](#).
- [27] M.Y. Liu, J.F. Wang, S.J. Zhu, Y.B. Zhang, Y.F. Sun, L.G. Wang, S.K. Guan, J Magn Alloys 8 (2020) 231–240, doi:[10.1016/j.jma.2019.09.009](#).
- [28] J.M. Wang, J. Wang, Q.Y. Fu, K. Sheng, M.Y. Liu, Y.F. Sun, D. Mei, Y.G. Kou, S.J. Zhu, S.K. Guan, Sci Technol (2021) 1–10, doi:[10.1080/1478422X.2021.1923178](#).
- [29] Y. Xiong, Z.Y. Yang, T. Zhu, Y.Y. Jiang, Mater Res Express 7 (2020) 015406, doi:[10.1088/2053-1591/ab648c](#).
- [30] Q. Wu, S.J. Zhu, L.G. Wang, Q. Liu, G.C. Yue, J. Wang, S.K. Guan, J Mech Behav Biomed Mater 8 (2012) 1–7, doi:[10.1016/j.jmbbm.2011.12.011](#).
- [31] P. Du, S. Furusawa, T. Furushima, J Magn Alloys 8 (2020) 614–623, doi:[10.1016/j.jma.2020.05.009](#).
- [32] J.F. Wang, Y.F. Zhou, Z.Y. Yang, S.J. Zhu, L.G. Wang, S.K. Guan, Mater Sci Eng C 90 (2018) 504–513, doi:[10.1016/j.msec.2018.05.005](#).
- [33] K.K. Guo, M.Y. Liu, J.F. Wang, Y.F. Sun, W.Q. Li, S.J. Zhu, L.G. Wang, S.K. Guan, J Magn Alloys 8 (2020) 873–882, doi:[10.1016/j.jma.2019.09.012](#).
- [34] P.H. Du, D. Mei, T. Furushima, S.J. Zhu, L.G. Wang, Y.F. Zhou, S.K. Guan, J Magn Alloys (2021), doi:[10.1016/j.jma.2020.12.015](#).
- [35] S.J. Zhu, Q. Liu, Y.F. Qian, B. Sun, L.G. Wang, J.M. Wu, S.K. Guan, Front Mater Sci 8 (2014) 256–263, doi:[10.1007/s11706-014-0259-3](#).
- [36] J. Wang, L.G. Wang, S.K. Guan, S.J. Zhu, C.X. Ren, S.S. Hou, J Mater Sci: Mater Med 21 (2010) 2001–2008, doi:[10.1007/s10856-010-4063-z](#).
- [37] L.Y. Huang, K.S. Wang, W. Wang, J. Yuan, K. Qiao, T. Yang, P. Peng, T.Q. Li, Eng Fail Anal 92 (2018) 392–404, doi:[10.1016/j.engfailanal.2018.06.012](#).
- [38] L.Y. Han, X. Li, C.L. Chu, J. Bai, F. Xue, Acta Metall Sinica 53 (2017) 1347–1356, doi:[10.11900/0412.1961.2017.00248](#).

- [39] J. Wang, V. Giridharan, V. Shanov, Z.G. Xu, B. Collins, L. White, Y. Jang, J. Sankar, N. Huang, Y. Yun, *Acta Biomater* 10 (2014) 5213–5223, doi:[10.1016/j.actbio.2014.08.034](https://doi.org/10.1016/j.actbio.2014.08.034).
- [40] D. Mei, S.V. Lamaka, X.P. Lu, M.L. Zheludkevich, *Corros Sci* 171 (2020) 108722, doi:[10.1016/j.corsci.2020.108722](https://doi.org/10.1016/j.corsci.2020.108722).
- [41] R.C. Zeng, J. Zhang, W.j. Huang, W. Dietzel, K.U. Kainer, C. Blawert, W. Ke, *Transactions of Nonferrous Metals Society of China* 16 (2006) s763–s771, doi:[10.1016/s1003-6326\(06\)60297-5](https://doi.org/10.1016/s1003-6326(06)60297-5).
- [42] Y. Zheng, Y. Li, J.H. Chen, Z.Y. Zou, *Corros Sci* 90 (2015) 445–450, doi:[10.1016/j.corsci.2014.10.043](https://doi.org/10.1016/j.corsci.2014.10.043).
- [43] J. Chen, M.R. Ai, J.Q. Wang, E.H. Han, W. Ke, *Corros Sci* 51 (2009) 1197–1200, doi:[10.1016/j.corsci.2009.02.020](https://doi.org/10.1016/j.corsci.2009.02.020).
- [44] G.F. Yang, Y.C. Kim, H.S. Han, G.C. Lee, H.K. Seok, J.C. Lee, *J Biomed Mater Res Part B* 103 (2015) 807–815, doi:[10.1002/jbm.b.33259](https://doi.org/10.1002/jbm.b.33259).
- [45] E. Merson, P. Myagkikh, V. Poluyanov, D. Merson, A. Vinogradov, *Mater Sci Eng: A* 748 (2019) 337–346, doi:[10.1016/j.msea.2019.01.107](https://doi.org/10.1016/j.msea.2019.01.107).
- [46] N. Winzer, A. Atrens, W. Dietzel, G. Song, K.U. Kainer, *JOM* 59 (2007) 49–53, doi:[10.1007/s11837-007-0104-6](https://doi.org/10.1007/s11837-007-0104-6).
- [47] J. Wang, Y. Jang, G. Wan, V. Giridharan, G.L. Song, Z. Xu, Y. Koo, P. Qi, J. Sankar, N. Huang, Y. Yun, *Corros Sci* 104 (2016) 277–289, doi:[10.1016/j.corsci.2015.12.020](https://doi.org/10.1016/j.corsci.2015.12.020).
- [48] Y. Zheng, Y. Li, J.H. Chen, Z.Y. Zou, *Corros Sci* 90 (2015) 445–450, doi:[10.1016/j.corsci.2014.10.043](https://doi.org/10.1016/j.corsci.2014.10.043).
- [49] X. Li, C.L. Chu, P.K. Chu, *Bioact Mater* 1 (2016) 77–84, doi:[10.1016/j.bioactmat.2016.09.002](https://doi.org/10.1016/j.bioactmat.2016.09.002).
- [50] D. Mei, S.V. Lamaka, J. Gonzalez, F. Feyerabend, R. Willumeit-Römer, M.L. Zheludkevich, *Corros Sci* 147 (2019) 81–93, doi:[10.1016/j.corsci.2018.11.011](https://doi.org/10.1016/j.corsci.2018.11.011).
- [51] D. Mei, S. Guan, *J Magn Alloys* 9 (6) (2021) 2225–2227, doi:[10.1016/j.jma.2021.11.002](https://doi.org/10.1016/j.jma.2021.11.002).
- [52] L. Cai, D. Mei, Z.-Q. Zhang, Y.-dd. Huang, L.-Y. Cui, S.-K. Guan, D.-C. Chen, M.B. Kannan, Y.-ff. Zheng, R.-C. Zeng, *J Magn Alloys* (2022), doi:[10.1016/j.jma.2022.02.005](https://doi.org/10.1016/j.jma.2022.02.005).